Immunohistochemical Evidence of Synaptic Retraction, Cytoarchitectural Remodeling, and Cell Death in the Inner Retina of the Rat Model of Oygen-Induced Retinopathy (OIR)

Allison Lindsay Dorfman,[1,2] *Nicolás Cuenca,*[3] *Isabel Pinilla,*[4] *Sylvain Chemtob,*[5,6,7] *and Pierre Lachapelle*[2]

Purpose. Postnatal exposure to hyperoxia destroys the plexiform layers of the neonatal rat retina, resulting in significant electroretinographic anomalies. The purpose of this study was to identify the mechanisms at the origin of this loss.

Methods. Sprague-Dawley (SD) and Long Evans (LE) rats were exposed to hyperoxia from birth to postnatal day (P) 6 or P14 and from P6 to P14, after which rats were euthanatized at P6, P14, or P60.

Results. At P60, synaptophysin staining confirmed the lack of functional synaptic terminals in SD (outer plexiform layer [OPL]) and LE (OPL and inner plexiform layer [IPL]) rats. Uneven staining of ON-bipolar cell terminals with mGluR6 suggests that their loss could play a role in OPL thinning. Protein kinase C(PKC)-α and recoverin (rod and cone ON-bipolar cells, respectively) showed a lack of dendritic terminals in the OPL with disorganized axonal projections in the IPL. Although photoreceptor nuclei appeared intact, a decrease in bassoon staining (synaptic ribbon terminals) suggests limited communication to the inner retina. Findings were significantly more pronounced in LE rats. An increase in TUNEL-positive cells was observed in LE (inner nuclear layer [INL] and outer nuclear layer [ONL]) and SD (INL) rats after P0 to P14 exposure (425.3%, 102.2%, and 146.3% greater than control, respectively [$P < 0.05$]).

Conclusions. Results suggest that cell death and synaptic retraction are at the root of OPL thinning. Increased TUNEL-positive cells in the INL confirm that cells die, at least in part, because of apoptosis. These findings propose a previously undescribed mechanism of cell death and synaptic retraction that are likely at the origin of the functional consequences of hyperoxia. (*Invest Ophthalmol Vis Sci.* 2011;52:1693–1708) DOI:10.1167/iovs.10-6197

Retinopathy of prematurity (ROP) remains a major cause of blindness in children despite many recent advances in neonatology, including clinical monitoring of oxygen administration in the neonatal intensive care unit and surgical treatments such as cryotherapy and laser photocoagulation.[1,2] Although ROP is considered a complex, multifactorial disease, gestational age and birth weight appear to be the most significant risk factors associated with its occurrence.[3–5] Interestingly, however, a number of studies have also provided evidence for a genetic basis for susceptibility to ROP and have revealed that sex, ethnicity, and ocular pigmentation might all play a role in contributing to the development of this disease.[6–10] However, differences in socioeconomic status have made it difficult to fully understand the relevance of ethnicity and genetics to the progression of ROP.[5]

The rat continues to be one of the most studied of all animal models of oxygen-induced retinopathy (OIR) because it offers the advantage of a highly immature retina at birth that is comparable to that of a 24- to 26-week-old human embryo.[11] Similar to what is observed in humans, exposure of the rat pup to postnatal hyperoxia will cause severe vasoconstriction and vaso-obliteration that are followed by an abnormal proliferation of retinal vessels on the return to room air,[12–15] all features that make it an elegant model with which to study the pathogenesis of OIR and to better understand the sequelae of ROP. Of interest, previous studies comparing pigmented and albino rats have shown that the former are less susceptible to ischemic retinal injury than the latter,[16] whereas others have demonstrated that certain pigmented strains develop more severe retinal neovascularization after hyperoxia.[17,18]

Although vascular impairments are considered the clinical hallmark of ROP, studies in our laboratory have been focused not only on retinal vasculature throughout hyperoxic exposure (retinal flatmounts) but also on the structural (retinal histology) and functional (rod-mediated and cone-mediated electroretinograms) features that characterize this model. Previous findings of ours have revealed that though structural and functional impairments are evident in the albino Sprague-Dawley rat (SD), including outer plexiform layer (OPL) thinning, reduced horizontal cell count, along with attenuation in amplitude of the b-wave of the electroretinogram (ERG) with relative sparing of the a-wave,[19–24] an even greater susceptibility of the pigmented Long Evans (LE) strain to hyperoxia was noted.[19] This

From the Departments of [1]Pharmacology and Therapeutics and [2]Ophthalmology/Neurology-Neurosurgery, McGill University-Montreal Children's Hospital Research Institute, Montreal, Quebec, Canada; the [3]Department of Physiology, Genetics and Microbiology, Facultad de Ciencias, Universidad de Alicante, Alicante, Spain; the [4]Department of Ophthalmology, University Hospital Lozano Blesa-Aragones Institute of Health Sciences, Zaragoza, Spain; and the Departments of [5]Pediatrics, [6]Ophthalmology, and [7]Pharmacology, University of Montreal, Montreal, Quebec, Canada.

Supported by Canadian Institutes of Health Research Grant MOP-13383; FRSQ-Réseau Vision; McGill University-Montreal Children's Hospital Research Institute; Ministerio de Ciencia e Innovación Grant BFU2009-07793/BFI; RETICS Grant RD07/0062/0012; Fundaluce; ONCE; Fundación Médica Mutua Madrileña (NC); and FIS Grant PS09/01854 (IP).

Submitted for publication July 12, 2010; revised September 22, 2010; accepted October 6, 2010.

Disclosure: **A.L. Dorfman**, None; **N. Cuenca**, None; **I. Pinilla**, None; **S. Chemtob**, None; **P. Lachapelle**, None

Corresponding author: Pierre Lachapelle, Department of Ophthalmology (D-164), McGill University-Montreal Children's Hospital Research Institute, 2300 Tupper Street, Montreal, Quebec, Canada, H3H-1P3; pierre.lachapelle@mcgill.ca.

extreme vulnerability is characterized by higher vascular dropout throughout hyperoxic exposure, permanently altered retinal function that occurs after all exposure regimens (even those limited to the first week of life), and permanently altered retinal structure that is limited not only to loss of the OPL and horizontal cells, as in SD rats, but that also extends into the inner retina, resulting in significant thinning of the inner nuclear layer (INL), inner plexiform layer (IPL), and ganglion cell layer (GCL).[19] Little is known, however, about the cytoarchitectural mechanisms that contribute to these findings.

The purpose of the present study was, therefore, to further investigate the impact of hyperoxia on retinal circuitry using confocal microscopy and immunohistochemical techniques to visualize retinal neurons to study synaptic contact, cell morphology, and cell death, which might contribute to these strain-specific differences.

METHODS

Animals

All experiments were performed in accordance with the ARVO Statement for the Use of Animals in Ophthalmic and Vision Research and were reviewed and approved by the McGill University-Montreal Children's Hospital Research Institute. Within 24 hours of birth, newborn litters of SD and LE rats (Charles River Laboratories, St. Constant, Quebec, Canada) were placed, with their mothers, in room air (21% O_2) or in a hyperoxic (80% O_2) environment (mixture of medical grade 100% O_2 and room air measured with an oxygen meter ($MaxO_2$ Ceramatec, model OM25-ME; Medicana Inc., Montreal, Canada). A controlled cyclic luminous environment (80 lux; 12 hours light/12 hours dark) was maintained throughout the exposure, and the temperature of the animal facility was kept at 23°C. Exposure to hyperoxia lasted for 22.5 hours daily and was interrupted for three periods of 0.5 hours at normoxia (21% O_2). Based on previous studies that suggested unequal susceptibilities to hyperoxia throughout developmental time points,[19,22,23] the hyperoxic cohort of each strain was divided at birth into three exposure protocols: from birth through postnatal day (P) 6 (LE, $n = 8$; SD, $n = 8$), birth through P14 (LE, $n = 8$; SD, $n = 8$), P6 through P14 (LE, $n = 8$; SD, $n = 8$). After hyperoxic exposure, groups of animals either were killed immediately for TUNEL labeling ($n = 4$ LE and 4 SD per exposure regimen, respectively) or were returned to room air (21% O_2) until P60 for retinal histology ($n = 4$ LE and 4 SD per exposure regimen, respectively). Data were compared with respective control groups raised in normoxic conditions (LE, $n = 8$; SD, $n = 8$). Finally, mothers of the litters were alternated between normoxic and hyperoxic conditions every 24 hours so that pulmonary complications known to arise in adult rats raised in a hyperoxic environment could be avoided.

Terminal Deoxynucleotidyl Transferase-Mediated dUTP Nick-End Labeling Assay

Animals were euthanatized immediately after removal from hyperoxia at P6 (after the P0-P6 exposure regimen) or at P14 (after the P0–P14 exposure regimen) ($n = 4$ LE and $n = 4$ SD per regimen) and were perfused intracardially with 4% paraformaldehyde (PFA) in 0.2 M phosphate buffer (PB; pH 7.4). After removal of the cornea and lens, eyecups were immersed in 4% PFA in 0.2 M PB (pH 7.4) (2 hours) and were cryoprotected in sequential sucrose solution gradients (10%, 20%, and 30% in PB for 30 minutes, 1 hour, and overnight, respectively) at 4°C. Eyecups were embedded the following day in optimal cutting temperature (OCT) compound (Tissue-Tek; Miles Laboratories, Elkhart, IN) and were frozen in a bath containing 2-methylbutane/liquid nitrogen. Cryosections (14-μm-thick) were collected on gelatin-coated slides on which TUNEL assays were conducted using an apoptosis detection kit (ApopTag Fluorescein In Situ Apoptosis Detection; Chemicon, Temecula, CA). TUNEL-positive cells were counted under a microscope (Axiophot; Zeiss, Jena, Germany) at 40× magnification attached to a digital camera (RR Slider Spot; Diagnostics Instruments, Inc., Sterling Heights, MI) with which images were captured. Results are expressed as mean ± SD.

Retinal Immunohistochemistry

After each hyperoxic regimen, animals were returned to room air until P60, at which point they were euthanatized with CO_2 ($n = 6–8$ SD and 6–8 LE per regimen). Eyes were enucleated, a small incision was made in the cornea, and the eyes were immersed in 4% PFA in 0.2 M PB (pH 7.4; 2 hours). The cornea and lens were then removed, after which eyecups were re-immersed in 4% PFA in 0.2 M PB (pH 7.4; 1 hour, 15 minutes) and washed in 0.1 M PBS before they were cryoprotected in sequential sucrose solution gradients (10%, 20%, and 30% in PB for 30 minutes, 1 hour, and overnight, respectively) at 4°C. Eyecups were subsequently embedded in OCT compound (Tissue-Tek; Miles Laboratories, Elkhart, IN) and were frozen in a bath containing 2-methylbutane/liquid nitrogen. Cryosections (14-μm-thick) were collected from the central retina on polylysine-S–coated slides for immunohistochemical analysis. To block any nonspecific binding, retinal sections were incubated in 10% normal goat serum (Jackson Laboratories, West Grove, PA). Without washing, they were then immunostained with single primary antibodies or with specific combinations of antibodies diluted in PBS containing 0.5% Triton X-100 (Table 1).

Retinal sections obtained from each of the normoxic and hyperoxic cohorts were incubated overnight at room temperature. The following day, they were washed in 0.1 M PBS and transferred to a cocktail of secondary antibodies to visualize antibody binding patterns, including either Alexa 488 goat anti-rabbit IgG or goat anti-mouse IgG and Alexa 555 goat anti-rabbit IgG or goat anti-mouse IgG secondary antibodies (Molecular Probes, Invitrogen, Eugene, OR).

TABLE 1. Antibodies Used for Immunostaining of Retinal Cells

Molecular Marker	Antibody (Reference)	Source	Working Dilution
Metabotropic glutamate receptor 6 (rod and cone ON-bipolar cells)	Rabbit anti-mGluR6[25–27]	Neuromics	1:3000
Calbindin D-28K (horizontal cells)	Rabbit polyclonal[28–30]	Swant	1:500
Protein kinase C, α isoform (rod ON-bipolar cells)	Mouse, clone MC5[30–32]	Santa Cruz Biotechnology	1:100
Protein kinase C, α isoform (rod ON-bipolar cells)	Rabbit polyclonal[30,31,33]	Santa Cruz Biotechnology	1:100
Parvalbumin (AII amacrine cells)	Rabbit polyclonal[26]	Swant	1:300
Recoverin (photoreceptor nuclei and cone bipolar cells)	Mouse monoclonal[34,35]	J.F. McGinnis, University of Oklahoma (Oklahoma City, OK)	1:2000
Synaptophysin (presynaptic marker of rod spherules and cone pedicles)	Mouse, clone SY38[36,37]	Chemicon	1:200
Transducin, Gαc subunit (cones)	Rabbit polyclonal[30,38]	Cytosignal	1:200
Bassoon (ribbon synapses)	Mouse monoclonal[39,40]	Stressgen	1:1000

All secondary antibodies were used at a 1:100 dilution in 0.1 M PBS 0.5% Triton X-100 for 1 hour. Finally, the sections were washed in 0.1 M PBS, mounted in watermount (Vector Laboratories, Burlingame, CA) and coverslipped for viewing with a confocal microscope (TCS SP2; Leica, Wetzlar, Germany). (See Figs. 1–8 and 10 for capture from the central retina, approximately 500 μm from the optic nerve. See Fig. 9 for capture from both the central [Figs. 9A, 9C, 9E] and the peripheral [from the ora serrata; Figs. 9B, 9D, 9F, 9G] retina.) To control for nonspecific staining, some sections were stained with the primary antibody omitted (Table 1).

Results

Recoverin

All photoreceptors in addition to cone bipolar subtypes 2 and 8[34] were labeled with antibodies against recoverin. The ONL in recoverin-stained sections from normoxic cohorts of LE and SD rats was approximately 12 to 14 cells thick (Figs. 1A, 1E, respectively). Although no significant changes could be identified with respect to the ONL and cone bipolar cells after

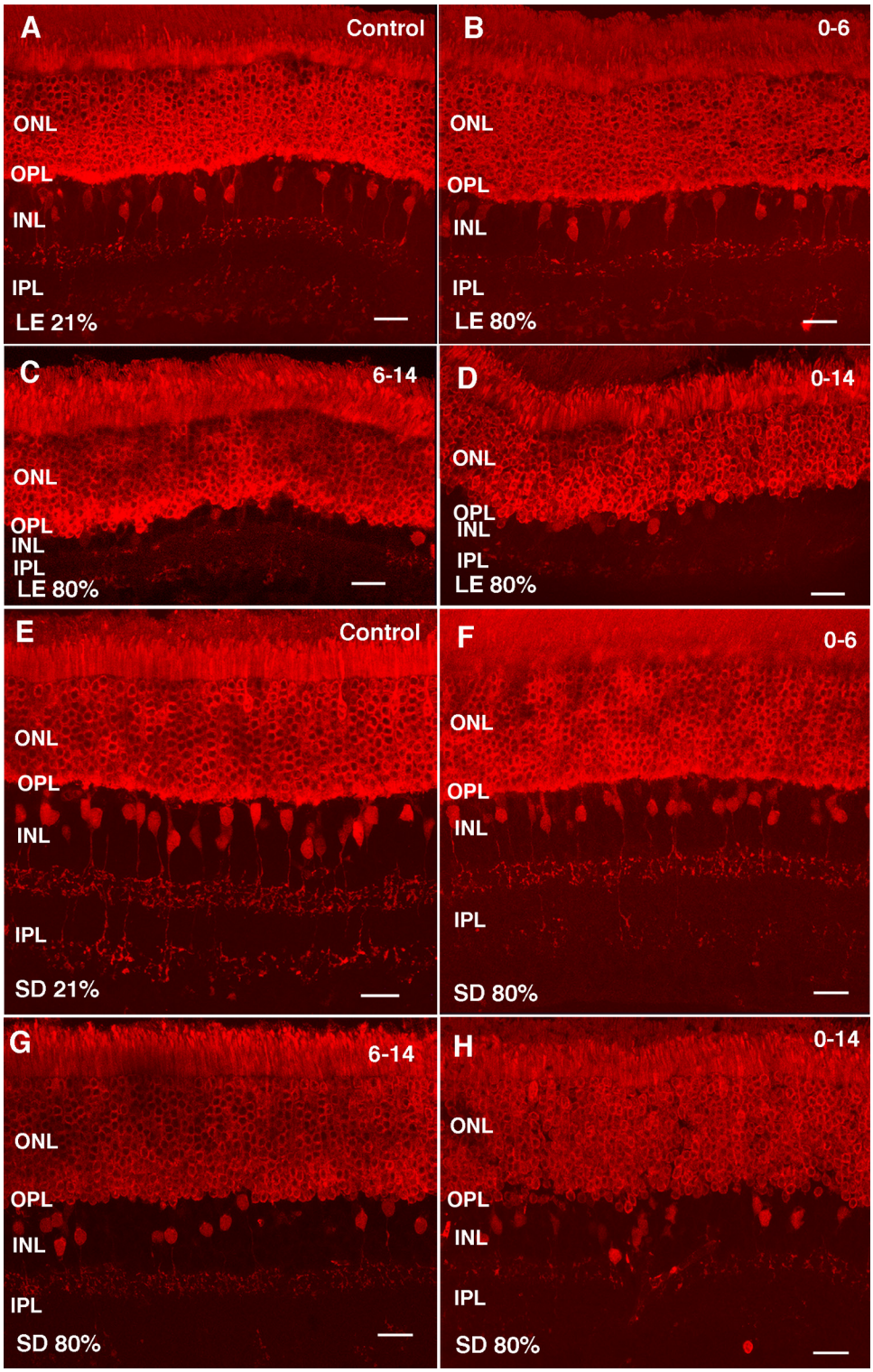

Figure 1. Anti-recoverin immunostaining of photoreceptors and types 2 and 8 cone bipolar cells in pigmented LE rats raised in normoxia (**A**) or hyperoxia from P0 to P6 (**B**), P6 to P14 (**C**), and P0 to P14 (**D**) and albino SD rats raised in normoxia (**E**) or hyperoxia from P0 to P6 (**F**), P6 to P14 (**G**), and P0 to P14 (**H**) at P60. Scale bars, 20 μm.

exposure from P0 to P6 in LE rats (Fig. 1B), thinning of the ONL to approximately eight to nine rows along with cone bipolar cell dropout was observed after exposures from P6 to P14 and P0 to P14 (Figs. 1C, 1D, respectively). The photoreceptor nuclei located in the inner part of the ONL lost their alignment, and there were obvious gaps at the level of the OPL.

Similar to what was observed in LE rats after exposure from P0 to P6, no significant morphologic alterations in the ONL or in cone bipolar cells could be noted in SD rats. The ONL cell number was intact after exposure from P6 to P14 (Fig. 1G) and P0 to P14 (Fig. 1H), with no suggestion of ONL thinning as was shown to occur in LE rats exposed to the same conditions (Figs. 1C, 1D). Loss of alignment of the ONL could be observed in SD rats after both exposure protocols (P6–P14, Fig. 1G; P0–P14, Fig. 1H), although changes were more evident in the P0 to P14 group (Fig. 1H).

Two types of cone bipolar cells with their somata located in the proximal row of the INL were labeled with antibodies against recoverin. Type 2 cone bipolar cells had large somata (Fig. 2A, arrows), and their axons ended in sublamina a of the IPL.[41] On the other hand, type 8 cone bipolar cells had small somata (Fig. 2A, arrowheads), and their axons descended through the IPL and ended in sublamina b of the IPL, close to the GCL.[41] A drastic reduction of both types of cone bipolar cells was observed after exposure from P6 to P14 and P0 to P14 in LE rats (Figs. 2C, 2D). After P6 to P14 exposure, loss of axon terminals in the a and b sublaminae of the IPL could be observed (Fig. 2C), and dramatic reductions of cone bipolar

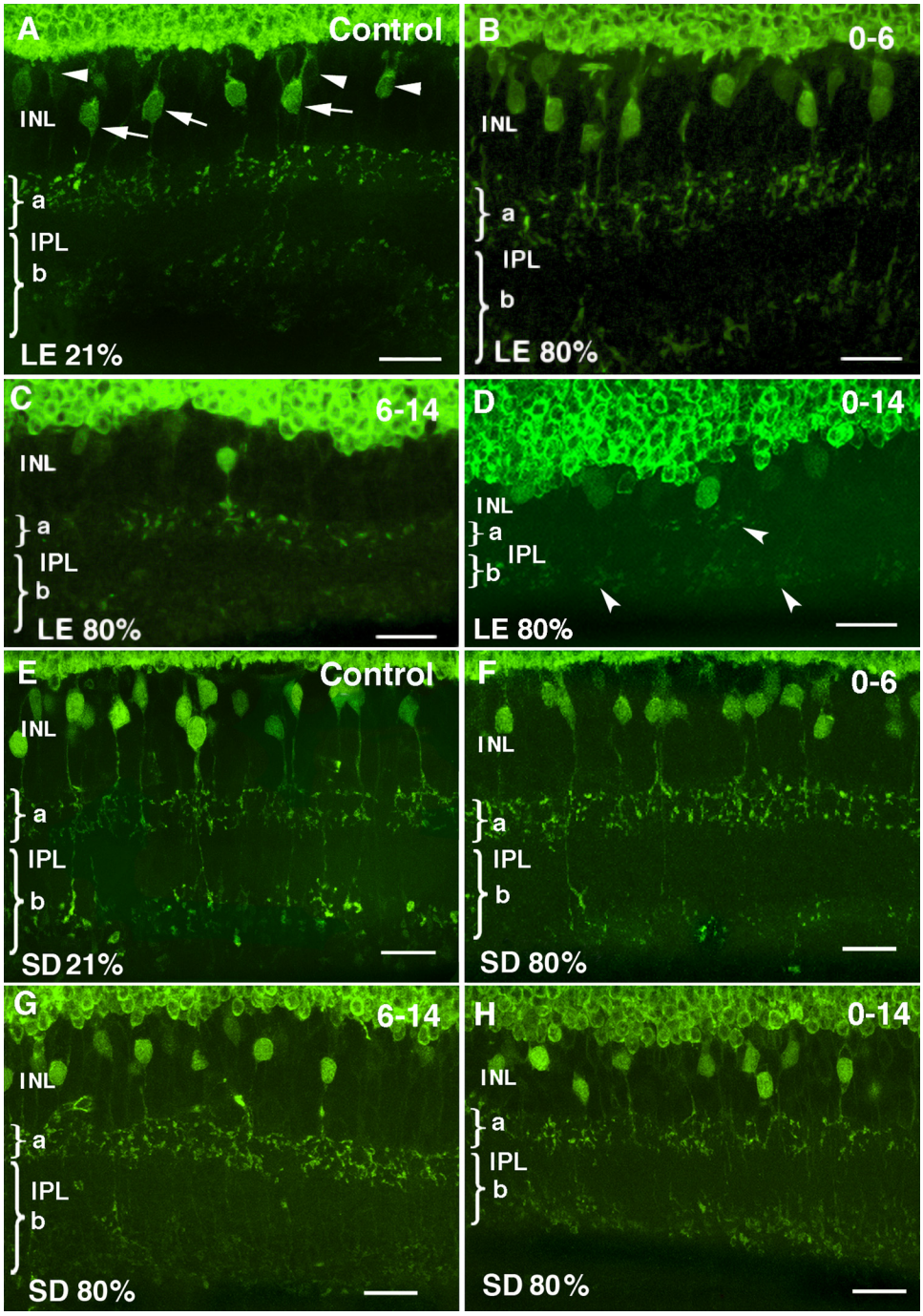

Figure 2. Two types of cone bipolar cells with their somata located in the proximal row of the INL are labeled with antibodies against recoverin in pigmented LE rats raised in normoxia (**A**) or hyperoxia from P0 to P6 (**B**), P6 to P14 (**C**), and P0 to P14 (**D**) and albino SD rats raised in normoxia (**E**) or hyperoxia from P0 to P6 (**F**), P6 to P14 (**G**), and P0 to P14 (**H**) at P60. Type 2 cone bipolar cells have large somata (**A**, *arrows*), and their axons end in sublamina a of the IPL. Type 8 cone bipolar cells have small somata (**A**, *arrowheads*), and their axons descend through the IPL and end in sublamina b of the IPL close to the GCL. Few identifiable cone bipolar cell terminals remain in the IPL of LE rats (**D**, *arrowheads*). Scale bars, 20 μm.

cell terminals could be evidenced, particularly in sublamina a of the IPL, after the P0 to P14 regimen (Fig. 2D, arrowheads). Although recoverin immunoreactivity in the ONL remained unchanged in SD rats after the P6 to P14 and the P0 to P14 regimens, there was evidence of cone bipolar cell dropout, albeit not to the same extent as that observed in LE rats (Figs. 2G, 2H). No differences in cone bipolar cell morphology could be observed between the P0 to P6 exposure regimen and control (Figs. 2E, 2F).

γ-Transducin

Cones are specifically labeled by antibodies against γ-transducin. In both strains, prominent γ-transducin immunoreactivity is seen in the cone outer and inner segments located in the photoreceptor layer, cell bodies located in the outer third of the ONL, axons, and pedicles (Figs. 3A, 3E). Disorganization of the pedicles in the OPL of LE rats was already evident after oxygen exposure from P0 to P6 (Fig. 3B). P6 to P14 and P0 to P14 regimens revealed a completely altered cone structure, with migration of the cone cell bodies to the center of the ONL in addition to synaptic retraction of cone bipolar cells in the inner retina, both of which occurred to a greater extent after maximal exposure (Figs. 3C, 3D). Cone inner segments and cone pedicles appeared to be truncated and disrupted compared with control. Furthermore, the cell bodies of bipolar cells stained with transducin were closer to the ONL than control and were clearly disorganized (Figs. 3C, 3D).

On the other hand, SD rats appeared to have a well-maintained retinal structure after exposure from P0 to P6 compared with control (Figs. 3E, 3F), and, though exposures that included the second week of life disrupted the normal cone pedicle organization leading to pedicle migration, the consequences were not as severe as those observed in LE rats (Figs. 3G, 3H). OPL thinning was evident in both SD and LE rats, but the ONL and cone lengths were clearly less affected in SD rats (see differences in ONL thickness between Figs. 3C and 3D and Figs. 3G and 3H).

Protein Kinase C-α

All rod bipolar cells are labeled with antibodies against protein kinase C (PKC)-α. In normoxic cohorts of LE and SD rats, rod bipolar cell dendritic terminals established connections with rod spherules in the OPL and their end-bulb axon terminals extended into the IPL (Figs. 4A, 4E).

Although only subtle changes in morphology could be observed in LE rats exposed from P0 to P6 (Fig. 4B), fewer bipolar cells could be identified after the P6 to P14 and the P0 to P14 exposure regimens. A dramatic loss of dendritic terminals in the OPL, along with fewer end-bulb terminals and lateral varicosities in the IPL, were evident in the remaining bipolar cells (Figs. 4C, 4D). Some of the remaining bipolar cell dendrites appeared flatter in rats that were maximally exposed to hyperoxia from P0 to P14, and there was a clear sprouting of the remaining dendrites into the ONL (Fig. 4D, arrows). These

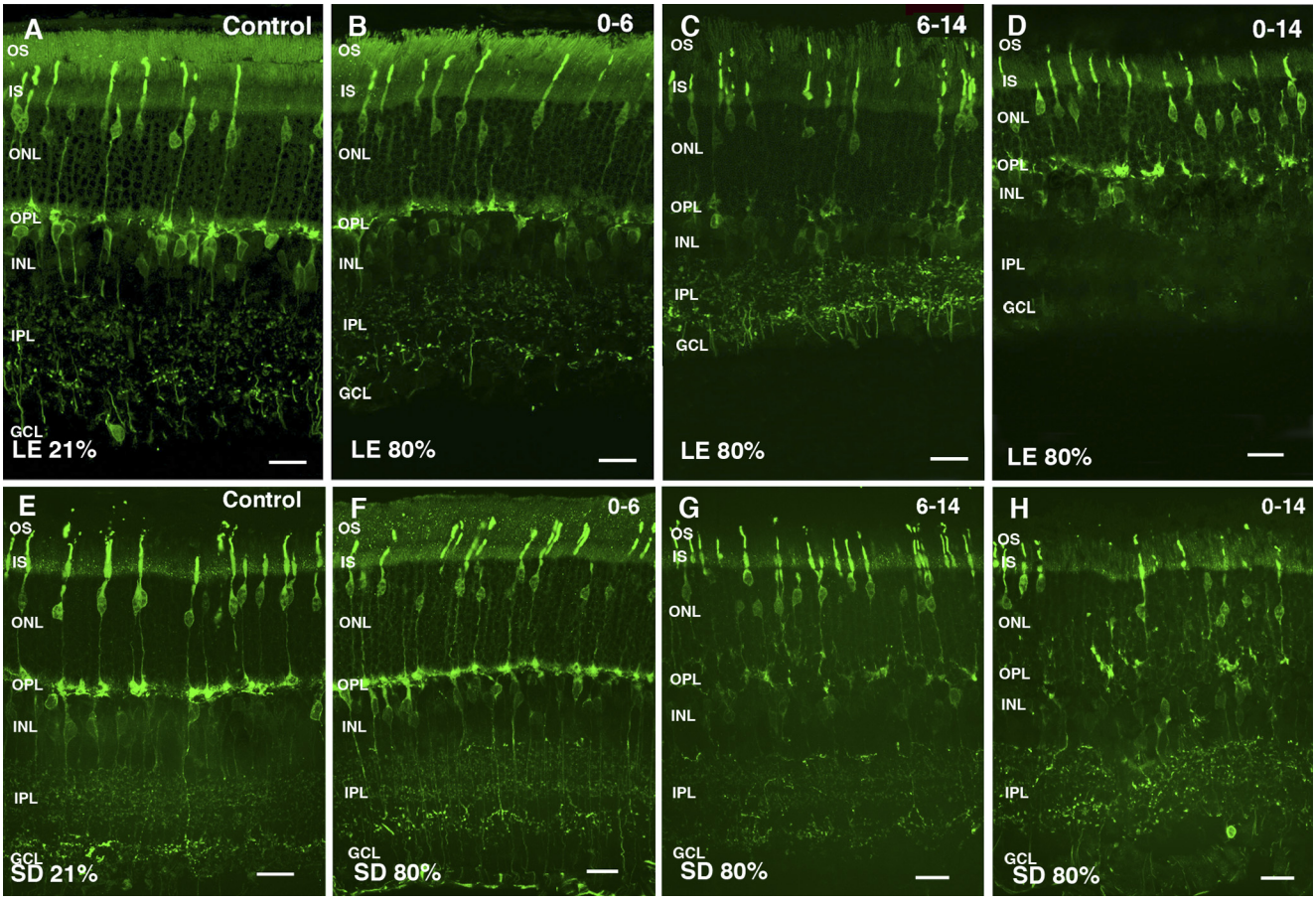

Figure 3. Cones are specifically labeled by antibodies against γ-transducin in pigmented LE rats raised in normoxia (**A**) or hyperoxia from P0 to P6 (**B**), P6 to P14 (**C**), and P0 to P14 (**D**) and albino SD rats raised in normoxia (**E**) or hyperoxia from P0 to P6 (**F**), P6 to P14 (**G**), and P0 to P14 (**H**) at P60. In both strains, prominent γ-transducin immunoreactivity is seen in the cone outer and inner segments located in the photoreceptor layer, cell bodies located in the outer third of the ONL, axons, and pedicles. Scale bars, 20 μm.

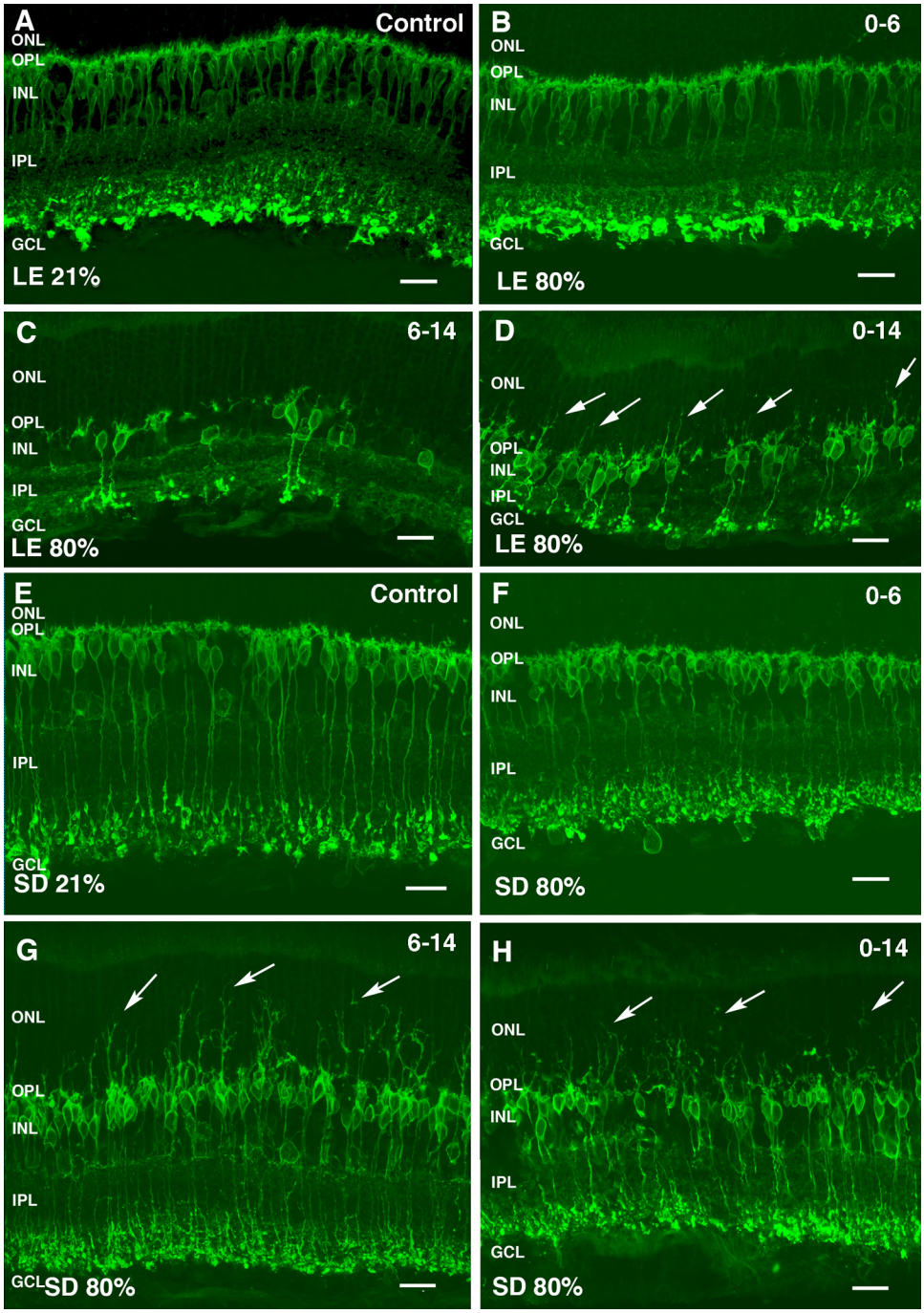

FIGURE 4. All rod bipolar cells are labeled with antibodies against PKC-α, which can be observed in pigmented LE rats raised in normoxia (**A**) or hyperoxia from P0 to P6 (**B**), P6 to P14 (**C**), and P0 to P14 (**D**) and albino SD rats raised in normoxia (**E**) or hyperoxia from P0 to P6 (**F**), P6 to P14 (**G**), and P0 to P14 (**H**) at P60. In normoxic cohorts of LE and SD rats, rod bipolar cell dendritic terminals establish connections with rod spherules in the OPL, and their end-bulb axon terminals extend into the IPL (**A**, **E**). Sprouting of the remaining bipolar cell dendrites into the ONL in LE rats is observed after exposure from P0 to P14 (**D**, *arrows*). Scale bars, 20 μm.

manifestations suggested impaired contact between photoreceptors and bipolar cells (most evident after the P0-P14 regimen), where bipolar cells appeared to be searching for contact with their presynaptic cells. Decreased PKC-α immunoreactivity was also evident in the axons and axon terminals of bipolar cells. The decreased length of the bipolar cells that occurred as a result of the manifestations described contributed to an overall decrease in retinal thickness (Figs. 4C, 4D).

Similar to LE rats, rod bipolar cell processes of SD rats exposed to hyperoxia from P0 to P6 maintained normal extension into the OPL and IPL (Fig. 4F). After exposure from P6 to P14 and P0 to P14, there was a clear sprouting of bipolar cell dendrites into the ONL (Figs. 4G, 4H). In addition, a reduction in length between the cell bodies and axon terminals of the rod bipolar cells could be observed, though PKC-α immunoreactivity in the axon terminals was relatively well preserved (Figs. 4G, 4H).

Synaptophysin

Figure 5 reveals an almost continuous layer of synaptophysin immunoreactivity in the OPL and IPL of both control LE and SD rats raised under normoxic conditions (Figs. 5A, 5E, respectively). After exposure to hyperoxia within the first week of life (P0–P6), LE rats reveal decreased synaptophysin staining in the OPL and IPL (Fig. 5B). Exposure from P6 to P14 resulted in a more punctate and discontinuous staining pattern in the OPL and a thinning of the IPL as evidenced by decreased levels of synaptophysin immunostaining (Fig. 5C). The most extreme damage to the OPL and IPL, however, was observed after

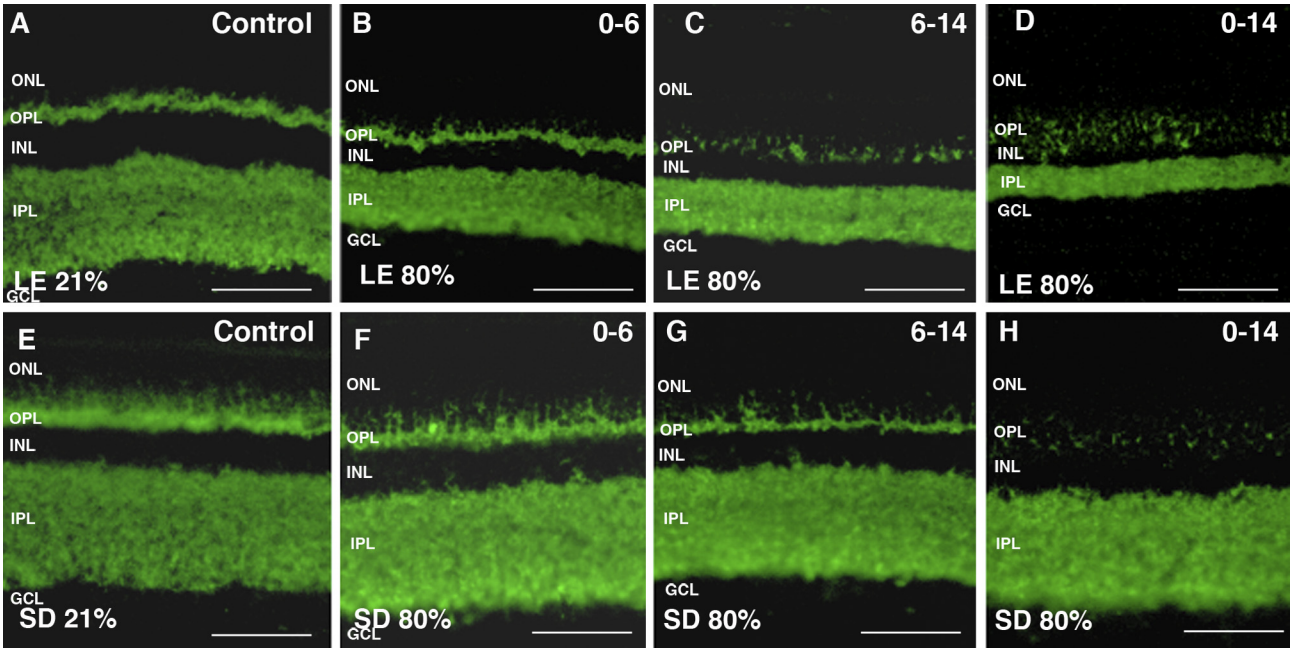

FIGURE 5. Anti-synaptophysin staining (presynaptic marker) located in the OPL and IPL of pigmented LE rats raised in normoxia (**A**) or hyperoxia from P0 to P6 (**B**), P6 to P14 (**C**), and P0 to P14 (**D**) and albino SD rats raised in normoxia (**E**) or hyperoxia from P0 to P6 (**F**), P6 to P14 (**G**), and P0 to P14 (**H**) at P60. Rats raised in normoxia (21% O_2; **A**, **E**) show intact synaptic terminals seen with continuous patterns of staining throughout both the OPL and the IPL. Rats exposed to hyperoxia show progressively more punctate staining in the OPL of LE and SD rats, whereas decreased synaptophysin staining in the IPL with increased exposure to hyperoxia is also evident in LE rats. Scale bars, 100 μm.

maximal exposure to hyperoxia from P0 to P14, where the most limited amount of synaptophysin staining could be evidenced (Fig. 5D).

Similar to LE rats, synaptophysin immunostaining progressively decreased in the OPL of SD rats beginning with early exposure that persisted throughout the first week of life (Fig. 5F). This continued to an even greater extent after exposure within the second week of life (Fig. 5G) and maximally to a completely thinned out OPL, where very weak immunostaining could be observed after exposure from P0 to P14 (Fig. 5H). In sharp contrast to LE rats, however, there was no evidence of any IPL changes in the SD hyperoxic cohorts compared with control, irrespective of the regimen (Figs. 5E–5H).

Calbindin and Bassoon

In the rat, dendrites of β-type horizontal cells contact with cone terminals, whereas their axons synapse with rod terminals. Antibodies against calbindin are used for horizontal cell labeling, and double immunolabeling with the antibody against the bassoon protein (a presynaptic protein that labels photoreceptor synaptic ribbon terminals in rod spherules and cone pedicles in the OPL) allows for their correlation with photoreceptor axon terminal distribution. This is best exemplified in Figure 6A, which shows paired structures between the synaptic ribbons of LE photoreceptor axon terminals labeled with antibodies against bassoon (red) and the terminal tips of horizontal cells labeled with calbindin antibodies (green; Fig. 6A, inset).

In LE and SD rats raised in a normoxic environment, horizontal cell processes were all associated with horseshoe-like bassoon immunoreactivity (Figs. 6A, 6E), which is suggestive of a normal pattern of contact between horizontal cell dendrites and photoreceptor synaptic ribbon terminals. Although no evidence of change in this regular pattern of staining could be observed in LE or SD rats after exposure for the P0 to P6 regimen (Figs. 6B, 6F), a decrease in calbindin immunoreactivity after the P6 to P14 and the P0 to P14 exposure regimens in both LE and SD rats (Figs. 6C, 6D and Figs. 6G, 6H, respectively) was indicative of a loss of horizontal cells and their processes, which inevitably contributes to reduced calbindin and bassoon pairing. It is of interest that despite the obvious decrease in horizontal cell terminals for the latter regimens, bassoon immunoreactivity, though clearly diminished, could be observed in the absence of any association with calbindin immunoreactivity (Figs. 6D, 6H, arrows). Sprouting in the ONL could be observed after P0 to P14 exposure in LE rats (Fig. 6D, arrowheads).

Bassoon and Metabotropic Glutamate Receptor 6 (mGluR6)

Antibodies against mGluR6 label the postsynaptic receptors on the dendritic tips of rod and cone ON-bipolar cells, and pairing can be observed between ON-bipolar cells and the synaptic ribbons of cone and rod terminals using double immunolabeling with mGluR6 and bassoon antibodies (Fig. 7). LE and SD control rats each revealed two types of pairing patterns between presynaptic and postsynaptic elements that are morphologically distinguishable but that were both present irrespective of strain. For example, Figure 7A reveals regions of pairing between mGluR6-stained (green) rod ON-bipolar cell dendrites and either bassoon-labeled (red) presynaptic rod spherules that have a horseshoe-like appearance (Fig. 7A, arrows) or bassoon-labeled presynaptic cone pedicles that take on more of a disc-like appearance (Fig. 7A, arrowheads). Presynaptic and postsynaptic pairing of rod-onto-rod bipolar cells was found in the outermost OPL, whereas that of cone-onto-cone bipolar cells was found in the innermost OPL of control LE and SD rats (Figs. 7A, 7E). Although evidence of some pairing could still be observed after exposure to hyperoxia from P0 to P6 in LE rats, rods synapsed less frequently with rod ON-bipolar cells, as shown by the presence of bassoon-stained rod terminals in the absence of association with mGluR6 in the outer OPL (Fig. 7B).

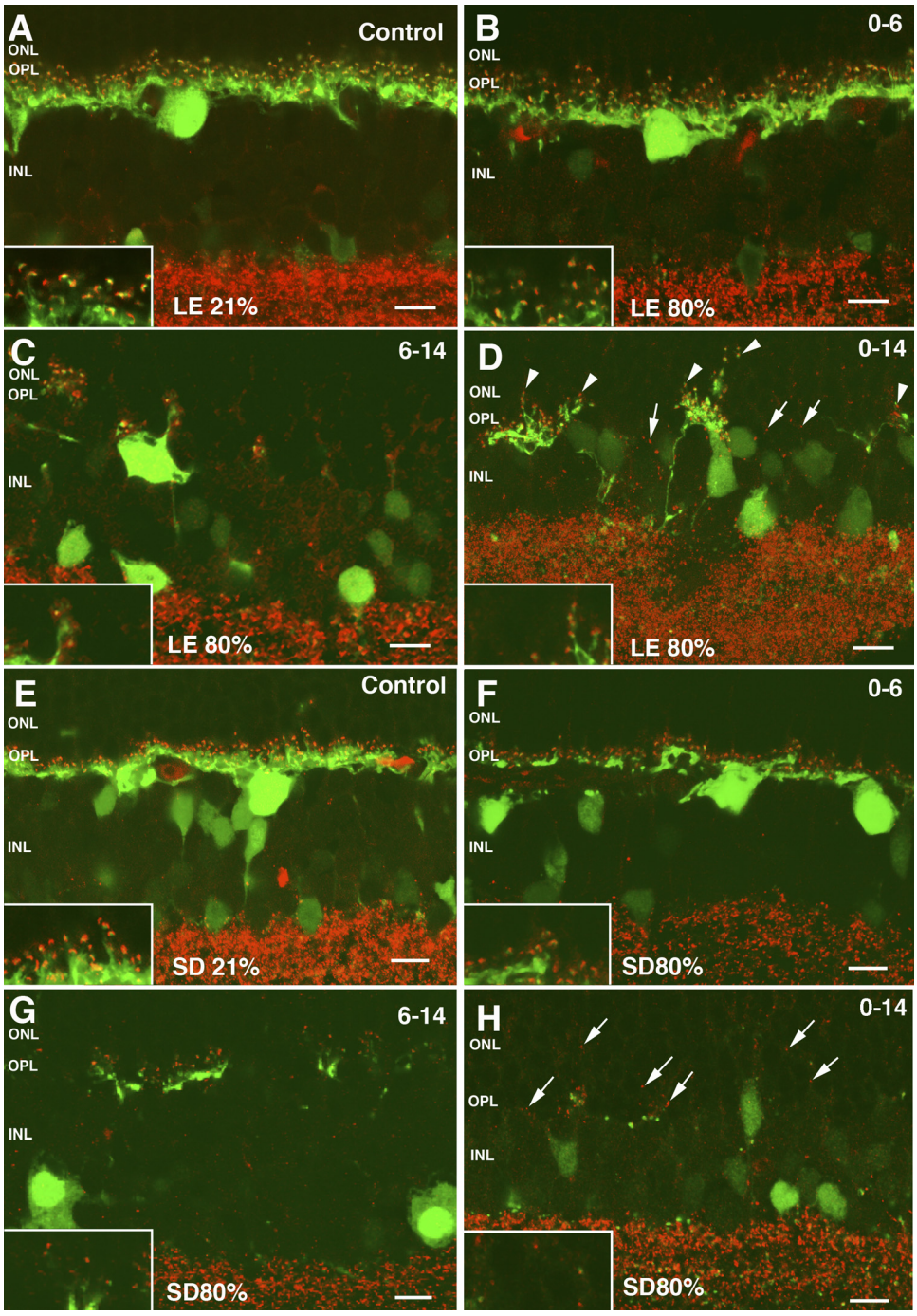

Figure 6. In the rat, dendrites of β-type horizontal cells contact with cone terminals, whereas their axons synapse with rod terminals. Antibodies against calbindin are used for horizontal cell labeling, and double immunolabeling with calbindin (*green*) and bassoon (*red*) labels β-type horizontal cells and photoreceptor synaptic ribbon terminals in rod spherules and cone pedicles in the OPL, respectively, in pigmented LE rats raised in normoxia (**A**) or hyperoxia from P0 to P6 (**B**), P6 to P14 (**C**), and P0 to P14 (**D**) and albino SD rats raised in normoxia (**E**) or hyperoxia from P0 to P6 (**F**), P6 to P14 (**G**), and P0 to P14 (**H**) at P60. Photoreceptor synaptic ribbon terminals are observed both in the absence of contact with horizontal cell processes (*arrows*) and paired with horizontal cell processes (*arrowheads*). Magnification of pairing between the synaptic ribbons of photoreceptor axon terminals labeled with antibodies against bassoon and the terminal tips of horizontal cells labeled with calbindin is shown (**A–H**, *insets*). Scale bars, 10 μm.

On the other hand, cone-onto-cone bipolar cell pairing took on more of a normal appearance and distribution in the inner OPL (Fig. 7B, arrowheads). mGluR6 immunoreactivity was distributed around cell bodies and axons of bipolar cells (Fig. 7B). Very infrequent pairing of bassoon and mGluR6 profiles were found in LE rats exposed to the P6 to P14 and the P0 to P14 regimens, where the OPL appeared to be completely disrupted (Figs. 7C, 7D). The bassoon staining that remained, however, was mostly limited to cone pedicles. Exposure of SD rats from P0 to P6 resulted in a reduction of immunoreactivity in the dendritic terminals of ON bipolar cells, whereas bassoon staining was observed in the absence of pairing with mGluR6-labeled profiles (Fig. 7F), similar to that in LE rats, albeit to a lesser extent. P6 to P14 and P0 to P14 exposure regimens revealed a complete disruption of the OPL with a near disappearance of synaptic terminals stained with mGluR6 and bassoon (Figs. 7G, 7H). Consequently, very limited pairing between photoreceptor terminals and bipolar cells could be seen.

PKC-α and Parvalbumin

In SD and LE rats, AII amacrine cells can be identified using an antibody to parvalbumin, a calcium-binding protein (Figs. 8A, 8E).[42–44] In normal rats, the AII amacrine cell bodies were located in the proximal part of the INL, adjacent to the IPL, and their processes extended to the different sublaminae of the IPL (Figs. 8A, 8E). Double labeling of parvalbumin with PKC-α reveals that the characteristic lobular appendages of AII amacrine cells are found in sublamina a of the IPL (Fig. 8A, arrow-

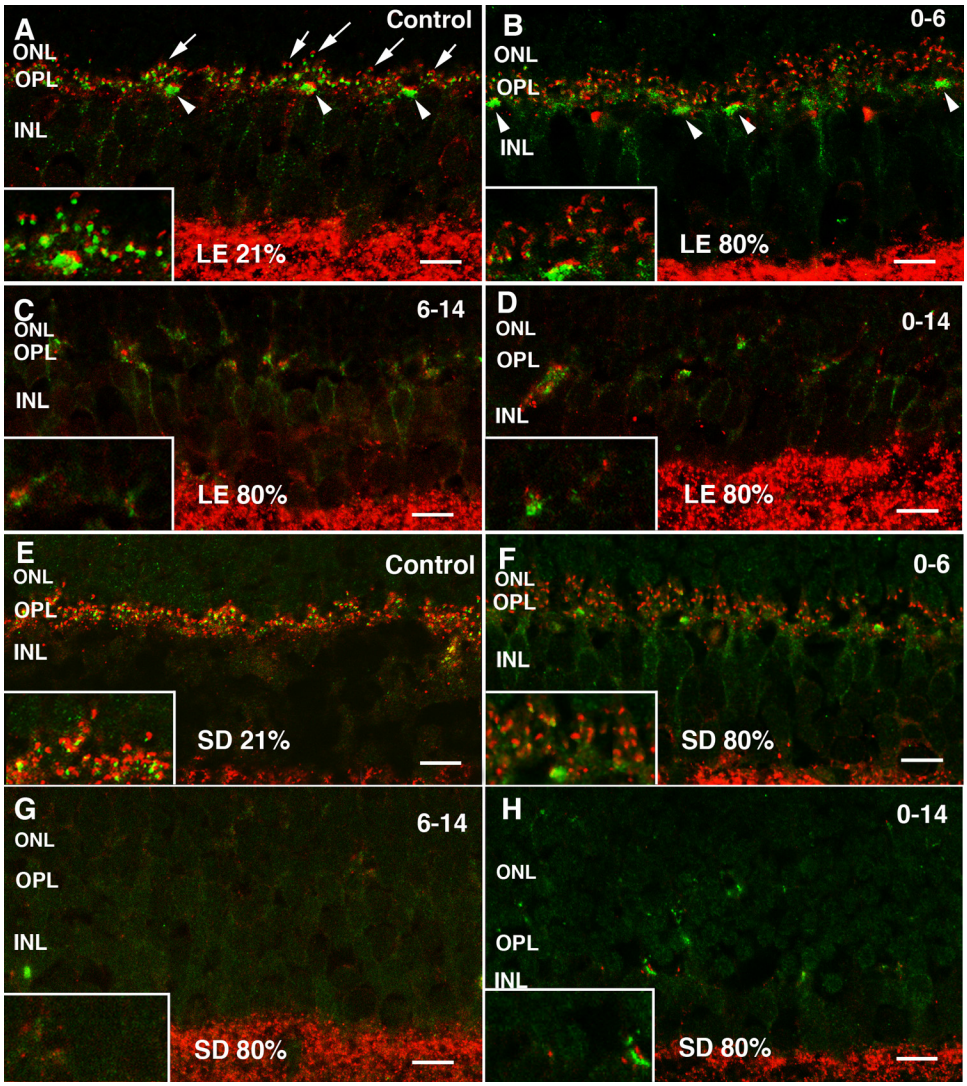

FIGURE 7. Double immunolabeling with mGluR6 (*green*) and bassoon (*red*) antibodies reveals pairing between ON-bipolar cells and the photoreceptor synaptic ribbon terminals in pigmented LE rats raised in normoxia (**A**) or hyperoxia from P0 to P6 (**B**), P6 to P14 (**C**), and P0 to P14 (**D**) and albino SD rats raised in normoxia (**E**) or hyperoxia from P0 to P6 (**F**), P6 to P14 (**G**), and P0 to P14 (**H**) at P60. Two types of pairing patterns between presynaptic and postsynaptic elements could be observed, namely pairing between mGluR6-stained rod ON-bipolar cell dendrites and either bassoon-labeled presynaptic rod spherules with a horseshoe-like appearance (**A**, *arrows*) or bassoon-labeled presynaptic cone pedicles that take on more of a disc-like appearance (**A**, *arrowheads*). Magnification of pairing between mGluR6-labeled ON-bipolar cells and bassoon-labeled photoreceptor synaptic ribbon terminals is shown (**A–H**, *insets*). Scale bars, 10 μm.

heads), and their dendrites extend into sublamina b to contact the axons of rod ON-bipolar cells (Fig. 8A, arrows).

After exposure of LE rats from P0 to P6, the dendritic processes of AII amacrine cells in the IPL became thinner and less numerous, losing their normal pattern of stratification. A reduction in contact between amacrine cell dendrites and the axon terminals of rod bipolar cells in sublamina b of the IPL was also noted (Fig. 8B, arrows). A dropout of AII amacrine cells and a loss of normal morphology of the remaining cells can be observed in LE rats exposed from P6 to P14 and P0 to P14. Finally, no areas of contact between AII amacrine cells and rod bipolar cell axons could be identified (Figs. 8C, 8D).

In the SD rat, the normal contact between AII amacrine cells and the axons of rod ON-bipolar cells (Fig. 8E, arrows) was maintained after exposure from P0 to P6 (Figs. 8F, arrows). On the other hand, the P6 to P14 and the P0 to P14 exposure regimens resulted in sprouting of rod ON-bipolar cells and limited contact between AII amacrine cell dendrites and rod ON-bipolar cell axons. Furthermore, their morphology in SD rats after these last regimens was abnormal and characterized by the loss of lobular appendages and dendrites in sublamina b of the IPL, though to a lesser extent than what was observed in LE rats because some areas of contact could still be identified between amacrine cells and rod ON-bipolar cells after these regimens (Figs. 8G, 8H, arrows).

Comparison between the Central and the Peripheral Retina

Irrespective of the oxygen exposure regimen used in LE rats, an overall preservation of the peripheral retina close to the ora serrata could be observed compared with the central retina, which was more susceptible to insult. Double immunolabeling with γ-transducin and recoverin reveals several morphologic changes in cones located in the central and the peripheral retina. For example, well-preserved cone outer segments can be identified in the peripheral retina, whereas those in the central retina are more disorganized. Moreover, their cell bodies are maintained in the outer layer of the ONL (as observed in control rats), and their axon terminals are also better preserved in the peripheral compared with the central retina. Finally, the inner plexiform layer in the peripheral retina is thicker than that of the central retina (Figs. 9A, 9B).

Double labeling with PKC-α and parvalbumin revealed that rod bipolar cells and AII amacrine cells were better preserved close to the ora serrata (Fig. 9D), maintaining the normal number and morphology of dendrites and axons compared with the central retina (Fig. 9C). Bassoon and calbindin immunostaining revealed that though few horizontal cells could be identified in the central retina, more could be observed closer to the ora serrata, similar to control retinas (Figs. 9E, 9F).

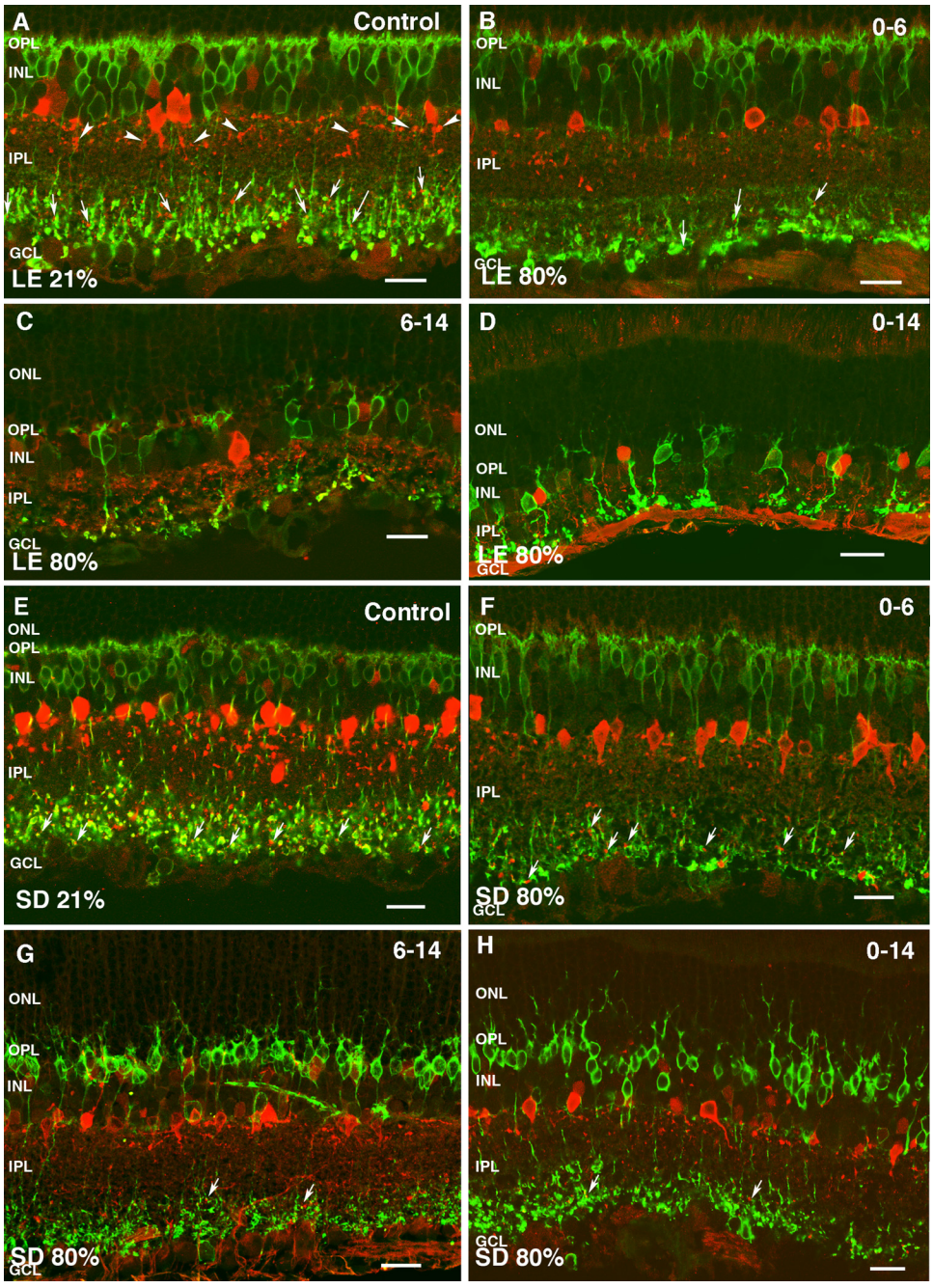

FIGURE 8. Double immunolabeling with parvalbumin (*red*) and PKC-α (*green*) reveals AII amacrine cells and rod bipolar cells, respectively, in pigmented LE rats raised in normoxia (**A**) or hyperoxia from P0 to P6 (**B**), P6 to P14 (**C**), and P0 to P14 (**D**) and albino SD rats raised in normoxia (**E**) or hyperoxia from P0 to P6 (**F**), P6 to P14 (**G**), and P0 to P14 (**H**) at P60. Characteristic lobular appendages of AII amacrine cells in sublamina a of the IPL (**A**, *arrowheads*) and dendrites of AII amacrine cells that extend into sublamina b of the IPL to contact the axons of rod ON-bipolar cells (**A**, **B**, **E**–**H** *arrows*) are observed. Scale bars, 20 μm.

Furthermore, pairing of horizontal cells with bassoon was also well preserved and more frequently observed in the peripheral compared with the central retina (Figs. 9E, 9F). Finally, the relationship between bassoon in the synaptic ribbon of the photoreceptor axon terminals and the postsynaptic receptor mGluR6 located on ON-bipolar cells could be identified only in the area close to the ora serrata (Fig. 9G, arrows), whereas very limited pairing could be observed elsewhere in the central retina (Fig. 9G). We could not identify any of these discrepancies between the central and the peripheral retina in SD rats after exposure to hyperoxia.

TUNEL

TUNEL staining was carried out in young rats immediately after hyperoxia to better understand the cellular death process occurring in the rat model of OIR. Staining was performed in LE and SD rats exposed to hyperoxia for 6 days (P0–P6; Figs. 10C, 10G, respectively) and 14 days (P0–P14); (Figs. 10D, 10H, respectively). Data were compared with control LE and SD retinas obtained at P6 (Figs. 10A, 10B, respectively) and P14 (Figs. 10E, 10F, respectively). Quantification of TUNEL-positive cells is shown in Figure 11. Although there was evidence of TUNEL-positive cells in both the ONL and the INL of LE rats after exposure to hyperoxia at P14, only the INL of SD rats revealed TUNEL-positive staining. Interestingly, a significant decrease in the number of TUNEL-positive cells could be observed after exposure to hyperoxia from P0 to P6 compared with respective normoxic cohorts in both LE (13.75 ± 3.40 compared with 42.25 ± 4.92, respectively; $P < 0.05$) and SD (13.33 ± 2.42 compared with 30.00 ± 2.00, respectively; $P < 0.05$) strains. These TUNEL-positive cells were not confined to any particular layer at P6 as observed at P14 following oxygen

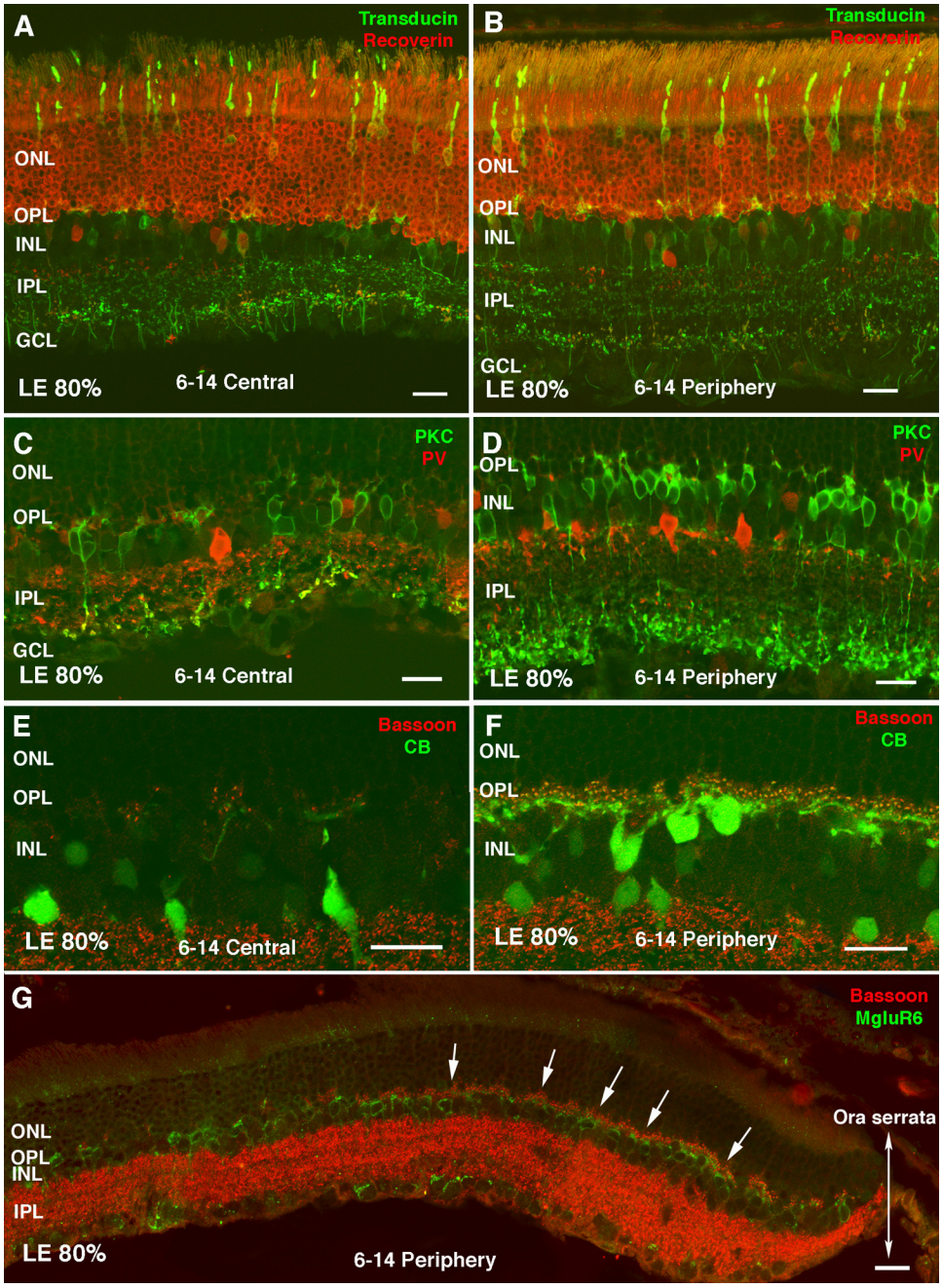

FIGURE 9. Comparison between central and peripheral retina in LE rats exposed to hyperoxia from P6 to P14. Double immunolabeling with transducin (*green*) and recoverin (*red*) (**A**, **B**), PKC-α (*green*) and parvalbumin (*red*) (**C**, **D**), bassoon (*red*) and calbindin (*green*) (**E**, **F**), and bassoon (*red*) and mGluR6 (*green*) (**G**) was used to indicate the differences in cell morphology in the central and peripheral retina, respectively. Areas of normal contact between bassoon-labeled photoreceptor synaptic ribbon terminals and mGluR6 labeled ON-bipolar cells near the ora serrata are shown (**G**, *arrows*). Scale bars, 20 μm.

exposure. In contrast, while TUNEL staining in the ONL of LE rats only tended to increase after maximal exposure from P0 to P14 compared with control (24.67 ± 3.22 compared with 12.20 ± 2.43, respectively; $P > 0.05$), a significantly higher number of TUNEL-positive cells was observed in the INL of LE rats compared with control (142.52 ± 29.61 compared with 27.13 ± 2.77, respectively; $P < 0.05$). Similarly, TUNEL-positive cells were significantly more numerous in the INL of SD rats exposed to hyperoxia (73.90 ± 3.39 compared with 30.00 ± 7.07, respectively; $P < 0.05$) after exposure from P0 to P14.

DISCUSSION

Previous studies of ours showed that postnatal exposure to hyperoxia results in vascular dropout, a permanently altered retinal structure as evidenced with histology and a permanently attenuated retinal function as evidenced with the ERG.[19–24] Our results suggested an even greater susceptibility of the pigmented LE rat to postnatal hyperoxia compared with the albino SD rat.[19] The purpose of the present study was to identify the mechanisms at the origin of these manifestations.

Our present study suggests that the inner retina is the primary target that is most significantly impacted by hyperoxic events, whereas damage to the outer retina can also be evidenced, but to a lesser extent. Furthermore, our findings confirm our previous report of increased susceptibility of LE rats to postnatal hyperoxia; irrespective of the exposure regimen, cytoarchitectural remodeling always occurred to a greater extent in this strain than in SD rats. Finally, the increased level of TUNEL-positive cells in the INL, particularly in LE rats, suggests that cells there die, at least in part, through apoptosis.

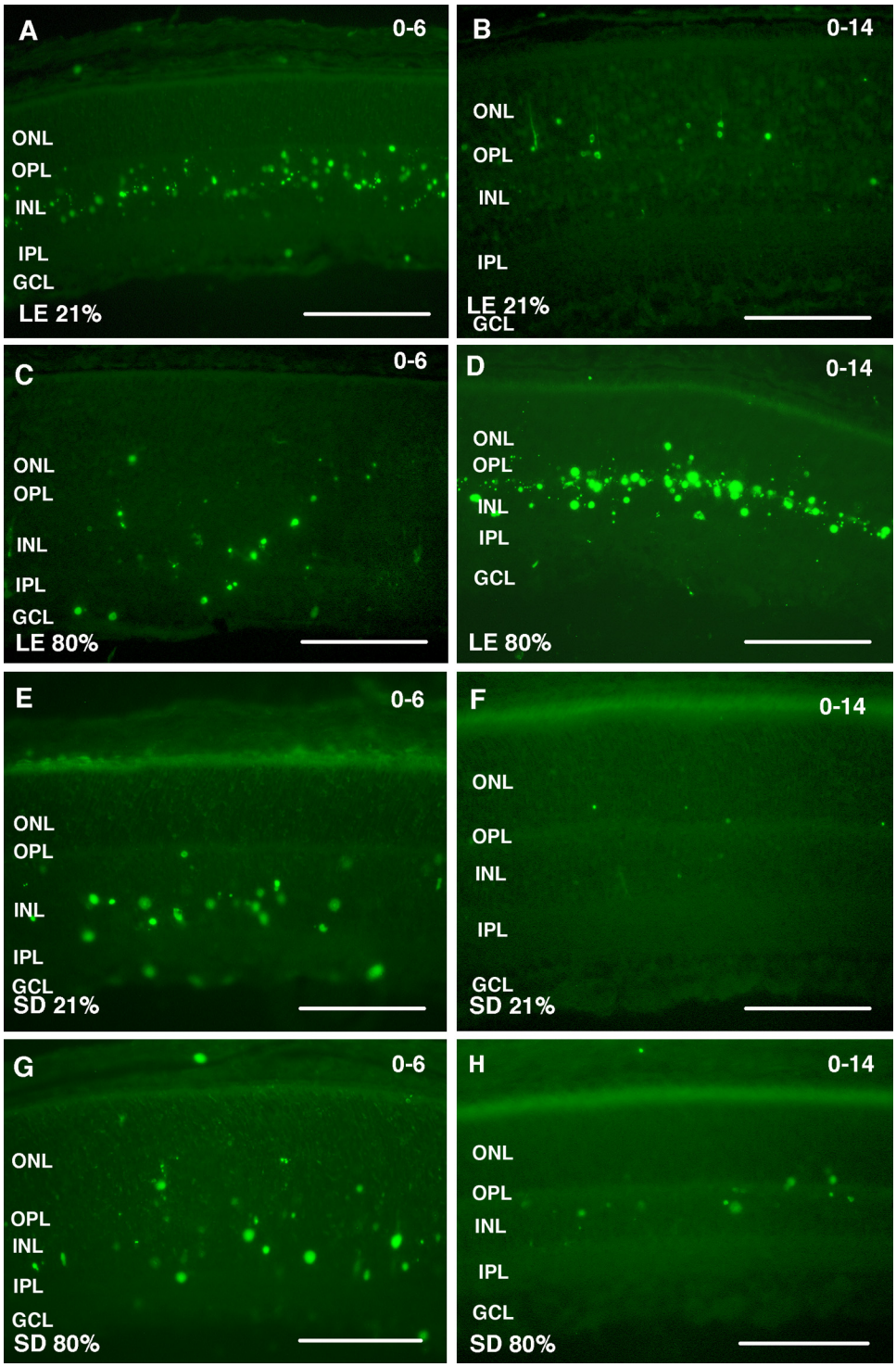

FIGURE 10. TUNEL staining was performed in LE and SD rats exposed to hyperoxia for 6 days (P0–P6; **C** and **G**, respectively) and 14 days (P0–P14; **D** and **H**, respectively). Data were compared with control LE and SD retinas obtained at P6 (**A** and **B**, respectively) and P14 (**E** and **F**, respectively). Scale bars, 100 μm.

As mentioned, one of the most striking structural consequences of postnatal hyperoxia involves the thinning to disappearance of the OPL, evidenced with retinal histology.[19–22,24] This suggested to us that a loss of synaptic contact between the photoreceptor layer and the inner retina would likely be responsible for the functional changes obtained with the ERG, namely attenuation of the b-wave amplitude with increasing oxygen exposure. Therefore, we used antibodies such as bassoon and synaptophysin (as presynaptic markers) and mGluR6 (a postsynaptic marker for ON-bipolar dendrites), for example, to further study synaptic contact at the OPL level. Our initial impressions were confirmed when we found a progressive decrease in synaptophysin staining, an integral membrane protein of synaptic vesicles that is expressed in all types of neurons and synapses in adult vertebrate retina[45] in the OPL of SD and LE rats and in the IPL of LE rats after exposure regimens that involved the second week of life, thus suggesting the lack of any functional synapses.

The synaptic markers associated with photoreceptors and processes of bipolar and horizontal cells show that significant abnormalities occur in the inner retina before photoreceptor damage, where bassoon staining can be seen in the absence of

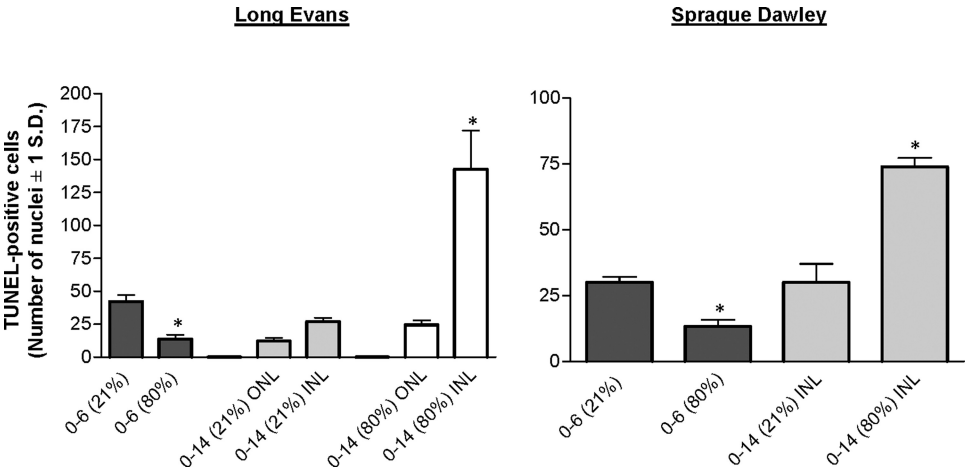

FIGURE 11. Graphic representation of the mean number of TUNEL-positive retinal cells in LE and SD rats exposed to hyperoxia for 6 days (P0–P6) and 14 days (P0–P14) compared with control LE and SD retinas obtained at P6 and P14. Statistically significant differences between age-matched normoxic and hyperoxic cohorts were found with Student's *t*-test ($P < 0.05$). $^*P < 0.05$, significantly different from control. Results are given as number of nuclei (mean ± 1 SD).

contact with mGluR6-stained ON-bipolar cells or calbindin-stained horizontal cells, for example (Figs. 6, 7). Furthermore, recoverin staining of the ONL and two types of cone bipolar cells reveals that thinning of the ONL (in LE rats), along with loss of normal ONL alignment (LE and SD rats), also occurs only once damage to the bipolar cells is evident, seemingly in response to a lack of cells to synapse with in the inner retina (Fig. 1). Finally, though the number of TUNEL-positive cells is significantly increased in the INL of both LE and SD rats after exposure from P0 to P14, they tend to increase only in the ONL of LE rats, suggesting limited cell death in this layer. In contrast, fewer TUNEL-positive cells were found in both LE and SD rat strains after exposure to hyperoxia from P0 to P6. Interestingly, apoptosis, or programmed cell death, has been suggested to play an important role in regulating the morphology and size of the developing retina. In fact, several apoptotic factors are expressed in high levels early in the retinal development of mice, for example,[46,47] and are downregulated with time. Consequently, it is not surprising that staining in control animals at P6 revealed the presence of a significant number of TUNEL-positive cells. Although it is difficult to delineate the different retinal layers of groups exposed to hyperoxia early in life (P0–P6), one wonders whether at this young age the normal early elimination of retinal cells is halted after exposure to hyperoxia, resulting in a significantly lower level of apoptotic cell death as part of an endogenous mechanism of cell survival and rescue in the developing retina. Of interest, previous findings in our laboratory using another model of environmental stress (exposure to bright light), namely the light-induced retinopathy model, revealed that though thinning of the ONL could be evidenced in juvenile rats (similar to adults, albeit to a lesser extent), a concomitant thickening of the INL was also observed.[48] It was suggested that this might occur as a compensatory mechanism to maintain normal retinal output in juvenile rats only because adult rats did not reveal similar findings. Reflecting the above are our findings of only minimal retinal function impairment for the same regimen of hyperoxic exposure,[19,22,23] whereas a window of increased susceptibility of retinal structure and function to postnatal hyperoxia exists for regimens that incorporate the second week of life.[19,23] Consequently, it is not surprising that significantly higher levels of cell death are observed after maximal exposure (P0–P14).

It is important to remember that the retina undergoes a period of intense maturation from birth until approximately P30, when it reaches both structural and functional maturity.[20] Consequently, this process must occur throughout both the hyperoxic (P0–P14) and the relative hypoxic phases (P15 and on) in the OIR model. Previous studies of ours also suggested a normal age-related decline in amplitude of scotopic and photopic ERG parameters between P30 and P60.[19–24,48] Interestingly, only the a-wave showed a similar age-dependent amplitude attenuation after exposure to hyperoxia, whereas the rod V_{max}, rod-cone b-wave, and photopic b-wave did not.[20] Similarly, findings obtained by Penn et al.[49] also revealed a decline in the scotopic b-wave amplitude (by ~40%) between control animals aged 5 and 9 weeks (P35–P63), but no similar attenuation was evident in the hyperoxic cohort, even at later time points (P112). In contrast, the a-waves obtained from the normoxic and hyperoxic groups within that age range were similarly attenuated. Collectively, these findings suggest that whereas normal developing animals are subjected to a progressive decline in retinal function, in addition to the normal thinning of the retinal layers between eye opening (~P15) through adulthood,[50] exposure to hyperoxia alters this process. This normal retinal thinning, which likely contributes to the observed functional attenuation with age, probably occurs through apoptotic mechanisms or as part of the normal aging process. Our previous findings,[20] therefore, suggest that because hyperoxia is of little consequence on the a-wave, photoreceptors are relatively well preserved and the normal cellular refinement of the outer retina that occurs with time (between P30 and P60) is not hampered under hyperoxic conditions. It is also of interest that, although delayed by 5 days, the maximum a-wave amplitude reached in hyperoxic rats is not significantly different from that reached in normal rats (attained at P19 in the normoxic cohort compared with P24 in the hyperoxic cohort). On the other hand, given the extreme damage generated by hyperoxia to the inner retina, which resulted in cellular dropout, reorganization of the inner retinal layers, and a severely depressed ERG b-wave, further deterioration of the retina with age was precluded. As early as P6, our results suggested a significantly lower number of apoptotic cells in the hyperoxic cohort compared with control (13.75 ± 3.40 vs. 42.25 ± 4.92; $P < 0.05$), suggesting that at this early stage of hyperoxic exposure, cells that would normally have died as a result of the normal maturation process likely survived to replace those that were affected by an excessively rich oxygen environment. This might also explain the decreased severity of the retinopathy we observed after early exposure (P0–P6) with respect to retinal function and structure.[19,22,23] After exposure until P14, this "rescue" phenomenon could no longer be observed whereby apoptotic cell death was significantly higher in hyperoxic cohorts (Figs. 10, 11). It has been shown that the rat retina exhibits an increased metabolic rate in the second to third week of life that is accompanied by a significant maturation phase.[51,52] Given that this enhanced metabolism has been associated with an increase in electron leaks in the mitochondria, thus leading to the facilita-

tion of free radical generation, one could hypothesize that the number of available cells initially able to replace those that succumb to the hyperoxic environment would no longer be available as a replacement because of the combined effect of hyperoxia and maturation. Consequently, this could lead to both the permanent structural consequences we are currently reporting along with the functional consequences that we have previously described.[19–24] Although the steps involved in this cascade of events remain to be fully understood, recent studies of ours have already begun to address the progressive evolution of the ultrastructural manifestations after the cessation of hyperoxia (at P15, P16, P17, P19, and P24) in SD[20] and LE rats (Dorfman A, et al. *IOVS.* 2010;51:ARVO E-Abstract 5590). Our ongoing studies are aimed at better understanding the relationship between normal cellular refinement throughout the retinal maturation process and progressive cell loss and reorganization throughout the initial hyperoxic stress and the return to normoxia.

Although our current findings suggest that apoptosis plays a role in cell death in the LE and SD models of OIR, one cannot rule out the possible contribution of necrotic cell death. Consequently, future studies aimed at investigating the possible contribution of necrosis to OIR are warranted to better understand the mechanisms of cell death in this model. Collectively, these findings of altered cell morphology suggest that the pathogenesis of OIR is initiated in the inner retina through bipolar cell dendrite retraction and is followed by damage (albeit less severe) to the outer retina.

Inner retina remodeling has previously been documented in other models of retinal degeneration in which morphologic changes can be observed in second-order neurons as a consequence of abnormal development or degeneration of the photoreceptors.[53] In contrast, our current findings suggest that the inner retina is the most important site of impact of postnatal hyperoxia. A further challenge in the photoreceptors of LE rats exposed to hyperoxia is the presence of melanin in the RPE, which, though believed to have a protective antioxidant effect in the retina,[4,5] can also take on the role of a pro-oxidant under conditions of environmental stress, thereby leading to cytotoxic activity such as photoreceptor damage.[54,55]

Interestingly, our findings of altered retinal morphology correlate with our previous documentation of functional impairment, as evidenced with the ERG.[19–24] The alterations in retinal cytoarchitecture we report here were likely at the root of the previously documented functional anomalies, such as the severe attenuation of the ERG b-wave that correlated with the morphologic deterioration and loss of bipolar cells. The a-wave, however, was always attenuated to a lesser extent, which also correlated with the relative preservation of photoreceptors. Furthermore, AII amacrine cells, which normally receive excitatory inputs from ON-rod bipolar cells in S5 of the IPL and transfer the rod signal to the cone pathway by means of conventional, chemical synapses with OFF-cone bipolar cells and gap junction-mediated electrical synapses with ON-type cone bipolar cells,[56] also reveal significant morphologic changes and decreased contact with rod ON-bipolar cells, thus further contributing to these findings.

Finally, the extreme susceptibility of the retinal cytoarchitecture of LE rats we report here has also been reflected in our findings of greater functional impairment in this strain, as evidenced by the a- and b-wave parameters of the ERG.[19] We have previously reported that the involvement of CNTF and FGF-2 may explain the preservation of photoreceptor function in SD rats.[19] For example, FGF-2 levels were found to be approximately twice as high in SD as in LE rats, and though CNTF levels were only significantly higher after exposure regimens that included the second week of life in LE rats, they were already significantly greater in SD rats after exposure within the first week (e.g., from P0 to P6).[19] The diffusion of various neurotrophic factors to the outer retina has been shown to occur after Müller cell gliosis in another model of environmental stress, namely exposure to a bright luminous environment.[57–59] Given that the INL in SD rats remains relatively more intact after hyperoxia than it does in severely compromised LE rats, one wonders whether a similar protective mechanism of photoreceptors might also occur in SD rats. Collectively, though structural and functional findings reveal that the inner retina is the most important target site of postnatal hyperoxia, our results suggest that the SD rat is better able to cope when faced with a hyperoxic challenge.

Although our present study was aimed at investigating the long-term consequences of OIR on retinal structure (at P60), previous findings of ours in the SD rat suggested that the pathophysiologic sequence of cytoarchitectural events was initiated while they were still in the hyperoxic regimen[20] given that the OPL thinning and the reduced HC count could be evidenced at the time of eye opening. Consequently, it is not surprising that there is no evidence of significant functional deficits, as determined by the ERG a-wave in the first 2 days or so after eye opening, though scotopic and photopic b-waves already tend to be attenuated in amplitude.[20] Our findings obtained at P60 suggest that the functional and structural impairments that ensued are permanent features of OIR and that OIR is initiated at a postreceptoral level, where both outer retinal structure and function remain intact, whereas synaptic impairment at the level of the OPL prevents signal transmission to the inner retina. Future studies aimed at understanding the short-term cytoarchitectural manifestations and the time course of the events in LE and SD rats with the use of techniques described herein will help to further elucidate the progression of the disease for each exposure regimen.

Given the important association that has been suggested to exist between postreceptoral neurons and retinal vasculature,[60] it is important to consider that impaired retinal vasculature might act as a potential contributing factor, thus influencing the integrity of the inner retinal neurons. Normally, retinal vascularization begins in the superficial inner retina by vasculogenesis, starting at the optic nerve and radiating outward from the posterior to the anterior retina, after which the vessels then invade the retina, thus forming intermediate and deep capillary beds.[61,62] The vaso-attenuation and microvascular degeneration that occur in a select number of retinal capillaries and then in larger groups of capillaries are key features of the pathophysiological process of OIR that precedes the pathologic neovascularization phase.[14,63,64] These are also characteristic of other ischemic retinopathies and reflect the normal response of the retinal tissue to meet its metabolic needs in an environment that is excessively rich in oxygen. The inability of the retinal vasculature to adequately extend from the inner retina place the OPL, horizontal cells, and bipolar cells—which are the most compromised structures in OIR—in the most vulnerable location furthest away from the "source" of retinal vasculature, thus offering another plausible explanation for their sensitivity to hyperoxia.

Interestingly, the extent of structural damage after hyperoxia was not found to be uniformly distributed in the retina of the LE rat. For example, though no discrepancies between the central and peripheral retina could be identified in SD rats after exposure to hyperoxia, the greatest consequences in LE rats were found in the central retina, with localized regions of normal synaptic contact and cell morphology in the peripheral retina. These findings come as a surprise, given that throughout the hyperoxic exposure, the central retina is that which is vascularized to a greater extent than the avascular peripheral retina; consequently, one would expect that the peripheral retina would be compromised to a greater extent on return to

normoxia (as a result of the avascular periphery) should OIR be considered primarily a vascular disease. Future studies aimed at better understanding the intraretinal blood supply in OIR are therefore warranted; one could expect to find a limited availability of central retinal vessels in the inner retina as a result of early microvascular degeneration, whereas revascularization throughout the neovascularization phase might be sufficient to maintain regions of normal structure and function in the peripheral retina. Of interest, significant deficits in amplitude and implicit time of the mfERG have also been identified in subjects whose clinical ROP symptoms resolved more than 10 to 20 years earlier.[65] Collectively, these findings suggest that a history of ROP (and OIR) can alter the development of the central retina and, consequently, the mfERG response it generates.

In conclusion, not only do present findings corroborate our previous demonstration of increased susceptibility of pigmented LE rats to postnatal hyperoxia compared with albino SD rats, they reveal previously undescribed mechanisms of synaptic retraction and cell death that are at the root of plexiform layer thinning. The increased number of TUNEL-positive cells in the nuclear layers after maximal exposure confirms that these cells die, at least in part, because of apoptosis and that LE rats are more susceptible than SD rats. Finally, our results point to the inner retina as the primary target of hyperoxic injury, after which damage to the outer retina occurs, though to a lesser extent. The mechanisms of cell death and synaptic retraction described herein are most probably at the origin of the functional consequences of hyperoxia. Future studies aimed at defining the time course of these events in both LE and SD rats, both throughout hyperoxic exposure and thereafter, are warranted. Finally, careful investigation of other factors, namely genetics and the role of melanin, might help to further elucidate the discrepancy between albino and pigmented strains, thereby furthering our understanding of the pathogenesis of OIR and ROP and the derivation of therapeutic modalities.

References

1. Holmström G, van Wijngaarden P, Coster DJ, Williams KA. Genetic susceptibility to retinopathy of prematurity: the evidence from clinical and experimental animal studies. *Br J Ophthalmol.* 2007; 91:1704–1708.
2. Holmström G. Retinopathy of prematurity. *BMJ.* 1993;307:694–695.
3. Brown BA, Thach AB, Song JC, Marx JL, Kwun RC, Frambach DA. Retinopathy of prematurity: evaluation of risk factors. *Int Ophthalmol.* 1998;22:279–283.
4. Monos T, Rosen SD, Karplus M, Yassur Y. Fundus pigmentation in retinopathy of prematurity. *Pediatrics.* 1996;97:343–348.
5. Shohat M, Reisner SH, Krikler R, Nissenkorn I, Yassur Y, Ben-Sira I. Retinopathy of prematurity: incidence and risk factors. *Pediatrics.* 1983;72:159–163.
6. Lang DM, Blackledge J, Arnold RW. Is Pacific race a retinopathy of prematurity risk factor? *Arch Pediatr Adolesc Med.* 2005;159:771–773.
7. Tadesse M, Dhanireddy R, Mittal M, Higgins RD. Race, *Candida* sepsis, and retinopathy of prematurity. *Biol Neonate.* 2002;81:86–90.
8. Saunders RA, Donahue ML, Christmann LM, et al. Racial variation in retinopathy of prematurity: the Cryotherapy for Retinopathy of Prematurity Cooperative Group. *Arch Ophthalmol.* 1997;115: 604–608.
9. Arnold RW, Kesler K, Avila E. Susceptibility to retinopathy of prematurity in Alaskan Natives. *J Pediatr Ophthalmol Strabismus.* 1994;31:192–194.
10. Schaffer DB, Palmer EA, Plotsky DF, et al. Prognostic factors in the natural course of retinopathy of prematurity: the Cryotherapy for Retinopathy of Prematurity Cooperative Group. *Ophthalmology.* 1993;100:230–237.
11. Weidman TA, Kuwabara T. Development of the rat retina. *Invest Ophthalmol Vis Sci.* 1969;8:60–69.
12. Patz A, Payne JW. Retinopathy of prematurity (retrolental fibroplasia). In: Tasman W, Jaegen EA, eds. *Duane's Foundations of Clinical Ophthalmology*. Philadelphia: Lippincott Williams & Wilkins; 1998:1–19.
13. Penn JS, Tolman BL, Henry MM. Oxygen-induced retinopathy in the rat: relationship of retinal nonperfusion to subsequent neovascularization. *Invest Ophthalmol Vis Sci.* 1994;35:3429–3435.
14. Reynaud X, Dorey CK. Extraretinal neovascularization induced by hypoxic episodes in the neonatal rat. *Invest Ophthalmol Vis Sci.* 1994;35:3169–77.
15. Moore A. Retinopathy of prematurity. In: Taylor D, ed. *Pediatric Ophthalmology*. Boston: Blackwell Scientific; 1990:365–375.
16. Safa R, Osborne NN. Retinas from albino rats are more susceptible to ischaemic damage than age-matched pigmented animals. *Brain Res.* 2000;862:36–42.
17. Gao G, Li Y, Fant J, Crosson CE, Becerra SP, Ma JX. Difference in ischemic regulation of vascular endothelial growth factor and pigment epithelium-derived factor in Brown Norway and Sprague Dawley rats contributing to different susceptibilities to retinal neovascularization. *Diabetes.* 2002;51:1218–1225.
18. Zhang D, Kaufman PL, Gao G, Saunders RA, Ma JX. Intravitreal injection of plasminogen kringle 5, an endogenous angiogenic inhibitor, arrests retinal neovascularization in rats. *Diabetologia.* 2001;44:757–765.
19. Dorfman AL, Polosa A, Joly S, Chemtob S, Lachapelle P. Functional and structural changes resulting from strain differences in the rat model of oxygen-induced retinopathy. *Invest Ophthalmol Vis Sci.* 2009;50:2436–2450.
20. Dorfman A, Dembinska O, Chemtob S, Lachapelle P. Early manifestations of postnatal hyperoxia on the retinal structure and function of the neonatal rat. *Invest Ophthalmol Vis Sci.* 2008;49: 458–466.
21. Dorfman AL, Dembinska O, Chemtob S, Lachapelle P. Structural and functional consequences of trolox C treatment in the rat model of postnatal hyperoxia. *Invest Ophthalmol Vis Sci.* 2006; 47:1101–1108.
22. Dembinska O, Rojas LM, Chemtob S, Lachapelle P. Evidence for a brief period of enhanced oxygen susceptibility in the rat model of oxygen-induced retinopathy. *Invest Ophthalmol Vis Sci.* 2002;43: 2481–2490.
23. Dembinska O, Rojas LM, Varma DR, Chemtob S, Lachapelle P. Graded contribution of retinal maturation to the development of oxygen-induced retinopathy in rats. *Invest Ophthalmol Vis Sci.* 2001;42:1111–1118.
24. Lachapelle P, Dembinska O, Rojas LM, Benoit J, Almazan G, Chemtob S. Persistent functional and structural retinal anomalies in newborn rats exposed to hyperoxia. *Can J Physiol Pharmacol.* 1999;77:48–55.
25. Cangiano L, Gargini C, Della Santina L, Demontis GC, Cervetto L. High-pass filtering of input signals by the Ih current in a non-spiking neuron, the retinal rod bipolar cell. *PLoS ONE.* 2007;12: e1327.
26. Cuenca N, Pinilla I, Sauvé Y, Wang S, Lu B, Lund RD. Regressive and reactive changes in the connectivity patterns of rod and cone pathways of P23H transgenic rat retina. *Neuroscience.* 2004;127: 301–317.
27. Nakajima Y, Iwakabe H, Akazawa C et al. Molecular characterization of a novel retinal metabotropic glutamate receptor mGluR6 with a high agonist selectivity for L-2-amino-4-phosphonobutyrate. *J Biol Chem.* 1993;268:11868–11873.
28. Barhoum R, Martínez-Navarrete G, Corrochano S, et al. Functional and structural modifications during retinal degeneration in the rd10 mouse. *Neuroscience.* 2008;26:155:698–713.
29. Oh EC, Khan N, Novelli E, Khanna H, Strettoi E, Swaroop A. Transformation of cone precursors to functional rod photoreceptors by bZIP transcription factor NRL. *Proc Natl Acad Sci U S A.* 2007;104:1679–1684.
30. Cuenca N, Pinilla I, Sauvé Y, Lund R. Early changes in synaptic connectivity following progressive photoreceptor degeneration in RCS rats. *Eur J Neurosci.* 2005;22:1057–1072.
31. Pinilla I, Cuenca N, Martínez-Navarrete G, Lund RD, Sauvé Y. Intraretinal processing following photoreceptor rescue by non-retinal cells. *Vision Res.* 2009;49:2067–2077.

32. Johnson J, Tian N, Caywood MS, Reimer RJ, Edwards RH, Copenhagen DR. Vesicular neurotransmitter transporter expression in developing postnatal rodent retina: GABA and glycine precede glutamate. *J Neurosci.* 2003;23:518–529.
33. Gong J, Jellali A, Forster V, et al. The toxicity of the PrP106–126 prion peptide on cultured photoreceptors correlates with the prion protein distribution in the mammalian and human retina. *Am J Pathol.* 2007;170:1314–1324.
34. McGinnis JF, Stepanik PL, Chen W, Elias R, Cao W, Lerious V. Unique retina cell phenotypes revealed by immunological analysis of recoverin expression in rat retina cells. *J Neurosci Res.* 1999; 55:252–260.
35. Chen W, Elias R, Cao W, Lerious V, McGinnis JF. Anti-recoverin antibodies cause the apoptotic death of mammalian photoreceptor cells in vitro. *J Neurosci Res.* 1999;57:706–718.
36. Martínez-Navarrete GC, Martín-Nieto J, Esteve-Rudd J, Angulo A, Cuenca N. Alpha synuclein gene expression profile in the retina of vertebrates. *Mol Vis.* 2007;13:949–961.
37. Zhang L, Fina ME, Vardi N. Regulation of KCC2 and NKCC during development: membrane insertion and differences between cell types. *J Comp Neurol.* 2006;499:132–143.
38. Zhang H, Li S, Doan T, et al. Deletion of PrBP/_ impedes transport of GRK1 and PDE6 catalytic subunits to photoreceptor outer segments. *Proc Natl Acad Sci U S A.* 2007;104:8857–8862.
39. Nagar S, Krishnamoorthy V, Cherukuri P, Jain V, Dhingra NK. Early remodeling in an inducible animal model of retinal degeneration. *Neuroscience.* 2009;160:517–529.
40. Pinilla I, Cuenca N, Sauvé Y, Wang S, Lund RD. Preservation of outer retina and its synaptic connectivity following subretinal injections of human RPE cells in the Royal College of Surgeons rat. *Exp Eye Res.* 2007;85:381–392.
41. Euler T, Wässle H. Immunocytochemical identification of cone bipolar cells in the rat retina. *J Comp Neurol.* 1995;361:461–478.
42. Endo T, Kobayashi M, Kobayashi S, Onaya T. Immunocytochemical and biochemical localization of parvalbumin in the retina. *Cell Tissue Res.* 1986;243:213–217.
43. Hamano K, Kiyama H, Emson PC, Manabe R, Nakauchi M, Tohyama M. Localization of two calcium binding proteins, calbindin (28 kD) and parvalbumin (12 kD), in the vertebrate retina. *J Comp Neurol.* 1990;302:417–424.
44. Cuenca N, Deng P, Linberg KA, Lewis GP, Fisher SK, Kolb H. The neurons of the ground squirrel retina as revealed by immunostains for calcium binding proteins and neurotransmitters. *J Neurocytol.* 2002;31:649–666.
45. Wiedenmann B, Franke WW. Identification and localization of synaptophysin, an integral membrane glycoprotein of Mr 38,000 characteristic of presynaptic vesicles. *Cell.* 1985;41:1017–1028.
46. O'Driscoll C, Donovan M, Cotter TG. Analysis of apoptotic and survival mediators in the early post-natal and mature retina. *Exp Eye Res.* 2006;83:1482–1492.
47. Wallace DM, Donovan M, Cotter TG. Histone deacetylase activity regulates apaf-1 and caspase 3 expression in the developing mouse retina. *Invest Ophthalmol Vis Sci.* 2006;47:2765–2772.
48. Joly S, Dorfman AL, Chemtob S, Moukhles H, Lachapelle P. Structural and functional consequences of bright light exposure on the retina of neonatal rats. *Doc Ophthalmol.* 2006;113:93–103.
49. Penn JS, Thum LA, Rhem MN, Dell SJ. Effects of oxygen rearing on the electroretinogram and GFA-protein in the rat. *Invest Ophthalmol Vis Sci.* 1988;29:1623–1630.
50. Cringle SJ, Yu PK, Su EN, Yu DY. Oxygen distribution and consumption in the developing rat retina. *Invest Ophthalmol Vis Sci.* 2006;47:4072–4076.
51. Graymore C. Metabolism of the developing retina, III: respiration in the developing rat retina and the effect of an inherited degeneration of the retinal neuro-epithelium. *Br J Ophthalmol.* 1960;44: 363–369.
52. Graymore C. Metabolism of the developing retina, 1: aerobic and anaerobic glycolysis in the developing rat retina. *Br J Ophthalmol.* 1959;43:34–39.
53. Pignatelli V, Cepko CL, Strettoi E. Inner retinal abnormalities in a mouse model of Leber's congenital amaurosis. *J Comp Neurol.* 2004;469:351–359.
54. Sarna T, Burke JM, Korytowski W, et al. Loss of melanin from human RPE with aging: possible role of melanin photooxidation. *Exp Eye Res.* 2003;76:89–98.
55. Sarna T. Properties and function of the ocular melanin—a photobiophysical view. *J Photochem Photobiol B.* 1992;12:215–258.
56. Kolb H. How the retina works. *Am Sci.* 2003;91:28–35.
57. Valter K, Bisti S, Gargini C, et al. Time course of neurotrophic factor upregulation and retinal protection against light-induced damage after optic nerve section. *Invest Ophthalmol Vis Sci.* 2005;46:1748–1754.
58. Wen R, Song Y, Cheng T, et al. Injury-induced upregulation of bFGF and CNTF mRNAS in the rat retina. *J Neurosci.* 1995;15: 7377–7385.
59. Faktorovich EG, Steinberg RH, Yasumura D, Matthes MT, LaVail MM. Photoreceptor degeneration in inherited retinal dystrophy delayed by basic fibroblast growth factor. *Nature.* 1990;347:83–86.
60. Fulton AB, Hansen RM, Moskowitz A, Akula JD. The neurovascular retina in retinopathy of prematurity. *Prog Retin Eye Res.* 2009;28: 452–482.
61. Gariano RF, Gardner TW. Retinal angiogenesis in development and disease. *Nature.* 2005;438:960–966.
62. Gogat K, Le Gat L, Van Den Berghe L, et al. VEGF and KDR gene expression during human embryonic and fetal eye development. *Invest Ophthalmol Vis Sci.* 2004;45:7–14.
63. Reynaud X, Hansen RM, Fulton AB. Effect of prior oxygen exposure on the electroretinographic responses of infant rats. *Invest Ophthalmol Vis Sci.* 1995;36:2071–2079.
64. Chan-Ling T, Tout S, Holländer H, Stone J. Vascular changes and their mechanisms in the feline model of retinopathy of prematurity. *Invest Ophthalmol Vis Sci.* 1992;33:2128–2147.
65. Fulton AB, Hansen RM, Moskowitz A, Barnaby AM. Multifocal ERG in subjects with a history of retinopathy of prematurity. *Doc Ophthalmol.* 2005;111:7–13.